Ahmad Momeni, Arezoo Ghadi*, Reza Fazaeli and Maryam Khavarpour

Synthesis, characterization, and optimization of a quaternary nanocomposite for efficient electromagnetic absorption coating in the X-band

https://doi.org/10.1515/ijmr-2021-8516 Received August 12, 2021; accepted August 17, 2022; published online June 30, 2023

Abstract: In this study, a quaternary composite of graphite, polyaniline, cobalt ferrite, and thermoplastic polyurethane as a shielding material was prepared. The composite materials were analyzed with X-ray diffraction, field emission scanning electron microscopy, vibrating-sample magnetometer and thermogravimetric analysis. The electromagnetic characterization of the samples was achieved using a Vector Network Analyzer in the X-band. The composites' conductivity was analyzed by using the four-point probe method. For the investigation of water absorption, the ASTM D570-98 Standard Method was used. Design-Expert software applied design optimization for broadband electromagnetic shielding of the composite film. Ultimately, we introduced a composite film as an efficient microwave absorbent that had a weight percentage of cobalt ferrite 6.95 %, polyaniline 20.04 %, graphite 12.13 %, and thermoplastic polyurethane 60.88 % in a thickness of 1.26 mm, which had shielding effectiveness higher than 30 dB, which was suitable for commercial purposes. The results showed that graphite played an essential role in increasing the composite's electrical conductivity and thermal stability but was unsuitable for water absorption resistance.

Keywords: Absorption loss; Conducting and magnetic materials; Electromagnetic interference shielding; Nanocomposite; Optimization.

1 Introduction

The excessive use of electromagnetic (EM) and electronic waves has led to severe problems, including pollution

and effects on human health and lives [1, 2]. Electromagnetic shielding has become more important with significant advances in stealth technology [3, 4]. The prevention of EM waves is achieved with reflection and absorption mechanisms, defined as shielding effectiveness (SE) [5, 6]. Based on past studies, two fundamental properties (magnetic and electrical) are needed to make a shielding material. They should have low heat loss, a broad absorption bandwidth, lightweight, thinness, wear resistance, excellent mechanical strength, and thermal stability [7, 8]. Carbon materials have been suggested as a way to make absorbents lighter and more effective. This is because they are very light-weight, have a high dielectric loss, and are very polarized [8, 9]. Graphite (G) is a pure, crystalline form of carbon with relatively weaker interlayer bonding than other carbon-based materials. Natural G is abundant and inexpensive and has been frequently employed in preparing composite materials as an electrical filler [10]. Previously published research has demonstrated that graphite powder decreases the penetration threshold [11]. Previous studies confirm the justification for using natural G to strengthen the microwave absorption properties and place graphite (a dielectric material) and some magnetic materials in a polymer [12, 13]. Moreover, ferrites are an effective magnetic absorbent material due to their high permeability, high microwave absorption capacity, and low cost [14]. However, ferrite as an absorbent is limited because of the narrow absorption bandwidth at GHz, low environmental resistance, and high density [15, 16]. When charge transfer between graphite and the intrinsically conductive polymers (ICP) occurs in composites, it leads to superior electrical conductivity [17]. An increase in G-polyaniline (PANI) composite conductivity with a specific ratio of G to PANI has shown that the electrical conductivity of the two-component composite was higher than that of the single components. Using the polymerization method, Li and others combined a triple composite (expanded G-PANI-Cobalt Ferrite). Their results showed that the electrical and magnetic properties of the ternary composite were better than those of the binary composites. The composite had a minimum reflection loss of -19.13 dB at 13.28 GHz at 0.5 mm thickness [18]. To increase electromagnetic interference (EMI) shielding,

^{*}Corresponding author: Arezoo Ghadi, Department of Chemical Engineering, Ayatollah Amoli Branch, Islamic Azad University, Amol, Iran, E-mail: arezoo.ghadi@gmail.com. https://orcid.org/0000-0002-2273-369X Ahmad Momeni and Maryam Khavarpour, Department of Chemical Engineering, Ayatollah Amoli Branch, Islamic Azad University, Amol, Iran Reza Fazaeli, Department of Chemical Engineering, South Tehran Branch, Islamic Azad University, Tehran, Iran

nanocomposites containing cobalt ferrite (CF), thermoplastic polyurethane (TPU), and fly ash were synthesized [19]. The results indicated that increasing the fly ash and CF contents increased electrical conductivity. These nanocomposites were used for EMI shielding at microwave frequencies from 0.1 to 20 GHz. From 0.1 to 8 GHz, the highest EMI shielding of 35 dB was achieved. Additionally, shielding effectiveness via absorbance was limited to 50 %. The core/shell composites (Fe₃O₄/C/PPy) were synthesized through hydrothermal and chemical oxidative polymerization techniques [20]. The highest shielding effectiveness total (SE_{T}) was achieved at 28 dB with 20 wt.% of Fe₃O₄/C as filler in the PPY as matrix and a thickness of 0.8 mm. Bertolini et al. [21] used melt mixing to prepare a TPU, polypyrrole, and carbon black composite. With a filler content of 15 wt.% and a thickness of 2 mm, the maximum SE_T in the X-band was 21.2 dB. Vaid et al. [22] used the melt mixing technique to prepare a ternarycomponent lightweight polyethylene composite containing CF and barium titanate. Composites with different proportions of filler (CF/barium titanate) in a polyethylene matrix were evaluated. The maximum SE_T value in the X-band and 2 mm thick was 17.9 dB with an 8 % filler content. Akhtar et al. [23] have assessed the microwave absorption properties of a three-layer absorber with optimized thickness. The tartrate-gel, Stober, and sol-gel methods were used to make the nanocomposites SrFe₁₂O₁₉, SiO₂@SrFe₁₂O₁₉, and MWCNTs@SrFe₁₂O₁₉, respectively. Resin epoxy was used as a matrix with a total thickness of 3 mm and a filler load of 15 % by weight for each layer. The highest reflection loss was achieved at -42 dB at 9.5 GHz with an effective bandwidth of 4.2 GHz. They show that this type of three-layer absorber is better for X-band absorption applications. In another study [24], a ternary nanocomposite (MWCNTs/CoFe₂O₄/FeCo) coated with a conductive polymer (PEDOT-PANI) was synthesized by microwave-assisted sol-gel followed by in-situ polymerization methods. Absorption characteristics were investigated in the frequency (12-18 GHz) Ku band. Nanocomposite with a 1.5 mm thickness had a maximum reflection loss of -90 dB at 13.8 GHz with a 4 GHz effective bandwidth. Akhtar et al. [25] Two different composites (Fe₃O₄/carbon fiber and Fe₃O₄/rGO) were uniformly incorporated into the resin epoxy matrix to get a single and double layer X-band absorber with 20 wt.% filler loading. The composites were made using the solvothermal method. According to the results, the minimum reflection loss values for every single layer of Fe₂O₄/carbon fiber and Fe₃O₄/rGO absorber were 15 dB (3 mm thickness and 1.5 GHz bandwidth) and 50 dB (3 mm thickness and 4 GHz bandwidth), respectively. The minimal reflection loss -52 was achieved by assembling a two-layer absorber

with Fe₃O₄/rGO composite on top and Fe₃O₄/carbon fiber composite on the bottom (total thickness of 2 mm and 4 GHz bandwidth). The results show that Fe₃O₄/rGO composite with high dielectric loss as an upper layer and Fe₃O₄/carbon fiber composite with high magnetic loss as a bottom layer can be used as a matching and absorber layer, respectively.

Previously, industrial applications of EM shielding composites have been hampered by many obstacles. The first problem was to control the composite's behavior at the output value (SE_T) throughout the frequency range. The second problem is that increasing these composites' dielectric loss (electric conductivity) decreases magnetic loss. The third problem, input variables' interaction, was not evaluated.

On the other hand, due to the complexity and difficulty of synthesizing quaternary composites, the primary research in the last two decades has been focused on the preparation of binary composites in industrial applications and especially on the preparation of ternary composites in the last five years. The improved electromagnetic shielding performance in binary composites was primarily due to improved impedance matching. Nonetheless, magnetic materials that decrease dielectric loss were a critical factor influencing electromagnetic shielding performance. If we desire to preserve high dielectric loss even after inserting different magnetic materials, another high dielectric loss material must be introduced into the absorbing materials (ternary composites). Nowadays, researchers have focused on the synthesis of quaternary composites. The benefit of quaternary composites over ternary composites is the presence of multiple interfaces; interfacial polarization plays a crucial role in EMI-preventing materials. Therefore, multiple interfaces in heterogeneous quaternary composites enhance the dielectric loss due to interfacial and space polarization and promote multiple reflections owing to their complicated morphologies. Although quaternary composites have several benefits, their synthesis is guite complicated, and hence there have been few studies. The innovation of this research is to solve the problems mentioned above.

On the other hand, most reports of past studies on microwave absorbent materials have highlighted high absorption at specific frequencies. However, weight, thickness, and wide-band absorption are critical in selecting an absorbing material. However, optimization of the properties of the absorbing material is challenging.

This work aimed to create a robust shielding material using a quaternary nanocomposite of CF, PANI, G, and TPU. The study looked at parameters including the thickness of the composite, the amount of filler in the composite, and the EMI shielding mechanisms over the X frequency range. Then, it used the response surface method (RSM) to make changes.

2 Experimental procedure

2.1 Materials

Ferrous sulfate heptahydrate (FeSO₄·7H₂O), aniline (C₆H₆NH₂) purity ≥99.5 %, cobalt chloride hexahydrate (CoCl₂·6H₂O) ≥99 %, sodium hydroxide (NaOH) ≥99 %, potassium nitrate (KNO₃) ≥99 %, ammonium persulfate $(NH_4)_2S_2O_8 \ge 98 \%$, hydrochloric acid (HCl) $\ge 35 \%$, tetrahydrofuran (THF) ≥99 % and graphite powder ≥97 % were purchased from Merck company and used without purification. TPU was purchased from the Epaflex Company (with Shore 85A).

2.2 Characterization

In this research, the phase structure of samples was analyzed by X-ray diffraction (XRD) (PHILIPS-PW 1730). Field emission scanning electron microscopy (FESEM) was used to investigate the surface morphology of the samples (MIRA3 TESCAN-XMU). The hysteresis loops of powders and films were determined at room temperature using a vibratingsample magnetometer (VSM) (LBKFB). An ultrasonic probe (UP400S-Hielscher) was employed during composite creation to disperse particles. For thermal analysis of the samples and measurement of both heat flow and weight changes in material, Thermogravimetric analysis (TGA) (Q600) was used. A four-probe electrical conductivity instrument (Huanyu-model) was used at room temperature. The ASTM D570-98 Standard Test Method was also performed to decide the water absorption percentage. The microwave wavelength absorption was examined in the X-band (8-12 GHz) by a Vector Network Analyzer (VNA) (HP-8410C). The samples were exposed in the X-band range and S_{11} and S_{12} (S-parameters are the electrical characteristics of a signal in a complex network) were established. Design-Expert software applied design optimization for broadband electromagnetic shielding of the composite film.

2.3 Experimental methods

2.3.1 Synthesis of CF: The advantages of the hydrothermal method, such as high efficiency, best controllability, ease of production, uniform product distribution, higher reaction rate, and no need for expensive and advanced equipment, led to the use of this synthesis method. 0.7 g FeSO₄ – 7H₂O and 0.35 g CoCl₂ – 6H₂O were added to 20 mL distilled water and stirred for 30 min on a magnetic stirrer. The mixture was placed in a stainless-steel autoclave and kept for three hours at 120 °C in the vacuum oven. Then, 0.4 g of KNO₃ and 0.9 g of NaOH were added to 18 mL of distilled water, and the mixture was placed on a magnetic stirrer for 20 min. The mixture was then placed into the autoclave and kept for six hours at 90 °C in the vacuum oven. Finally, the mixture was rinsed with distilled water several times and dried for two hours at 100 °C.

2.3.2 Synthesis of PANI/CF/G: Different amounts of aniline were mixed with 50 mL of HCl (1M) and placed in an ice bath for 15 min.

Different CF and G powder ratios are produced by mixing CF at 2, 6, and 10 wt.% with G powder at 5, 10, and 15 wt.% was added to the previous mixture and stirred in an ice bath for one hour. Next, 1.7 g of (NH₄)₂S₂O₈ was added to 37.5 mL of distilled water. All the mixtures were then added together dropwise. Eventually, the mixture was washed several times with distilled water and placed in an oven for 3 h at 60 °C.

2.3.3 Preparation of TPU/PANI/CF/G: Because of the better dispersion of the particles, the solution blending method was used. TPU was added at a concentration of 54-73 wt.% to 20 mL of THF and left at room temperature for 24 h. Different amounts of PANI/CF/G were added to the previous solution and placed on a magnetic stirrer for 24 h. The mixture was then placed under sonication for 40 min. The samples were then poured into 1, 1.5, and 2 mm thick molds. After 24 h of evaporating the solvent, the composites were separated from the molds.

The preparation of the TPU/PANI/CF/G flowchart is included in Figure S1.

3 Results and discussion

3.1 X-ray diffraction

XRD patterns for CF, CF/PANI, CF/PANI/G, and CF/PANI/G/TPU are shown in Figure 1a. The CF nanoparticles were assigned by the standard (JCPDS no. 00-022-1086). The observed peaks at $2\theta = 21.24$, 35.10, 41.4, 50, 62.2, 67.5, and 74.8° were assigned (111), (220), (311), (400), (422), (511), and (440) respectively, with an inverse cubic spinel structure with space group [26]. The XRD pattern of PANI had broad peaks at $15-30^{\circ}$ and peaks at $2\theta = 15.45, 20.45, 25.45, and <math>25.9^{\circ}$, which is similar to PANI. Two peaks were observed in the XRD pattern of CF/PANI/G at 26.45° (large) and 54.7° (small), which confirms the presence of G in the nanocomposite [27, 28]. Based on the results, the broad peak in the 15 $< 2\theta < 30$ was increased because TPU and PANI had a higher percentage by weight than other materials. Besides the peaks above,

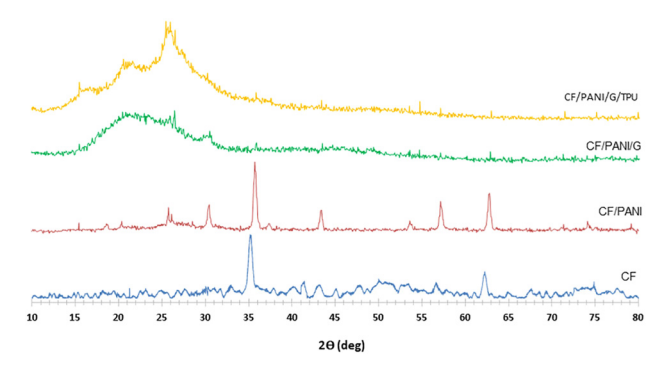


Figure 1: XRD patterns of cobalt ferrite-cobalt ferrite/polyaniline-cobalt ferrite/polyaniline/graphite and cobalt ferrite/polyaniline/graphite/ thermoplastic polyurethane.

there was a peak at 20.55° , which matched TPU [29]. By using X'pert Highscore software and the Williamson–Hall method the following qualitative and quantitative results were obtained. The output parameters were; Crystal system (Rhombohedral) – Space group ($R\overline{3}m$) Space group number (166) – a (Å): 5.9366 - b (Å): 5.9366 - c (Å): 14.5430 – Alpha (°): 90.0000 – Beta (°): 90.0000 – Gamma (°): 120.0000 – Crystallite size (nm) = 131.

3.2 Morphological characterization

The FESEM technique was used to determine the particle morphology. Based on the results, the morphology of the CF nanoparticles was octahedral with 50–150 nm (Figure 3a). In Figure 2b, PANI surrounds the CF nanoparticles. Figure 2c shows CF/PANI/G. The morphology of the composites shows clustering and layering. In Figures 2d and e FESEM images for TPU/PANI/CF/G are shown on 2 μm and 200 nm scales. The filler particles have a distribution of 50–100 nm in the TPU matrix, despite the magnetic property of CF, which leads to agglomeration.

3.3 Magnetic properties

The magnetic measurements of CF, PANI/CF, PANI/CF/G, and TPU/PANI/CF/G composites were performed using a vibrating sample magnetometer (VSM) hysteresis loop recorded at room temperature, as shown in Figure 3. CF's saturation magnetization (M_s) , 57.89 emu g, almost matches a previous report [30]. CF's coercivity (H_c) was recorded at 493 Oe, and remanent magnetization (M_r) was 13.06 emu g⁻¹. " M_s " and " M_r " of PANI/CF were 18.31 and 10.78 emu g⁻¹, respectively, and coercivity was 1910 Oe. The interaction between CF and PANI led to a significant decrease in the magnetic properties of the nanocomposite, which matches a previous report [31]. For PANI/CF/G, M_s and M_r were 4.92 and 1.11 emu g⁻¹, respectively. Also, coercivity was 490 Oe. Magnetic saturation was further decresed by G because it is a diamagnetic material [32]. The CF had an intense ferromagnetic phase, so the hysteresis diagram for PANI/CF/G showed the same state.

The quaternary composite had an M_s of 1.03 emu g⁻¹ and remanent magnetization of about 0.3 emu g⁻¹. Also,

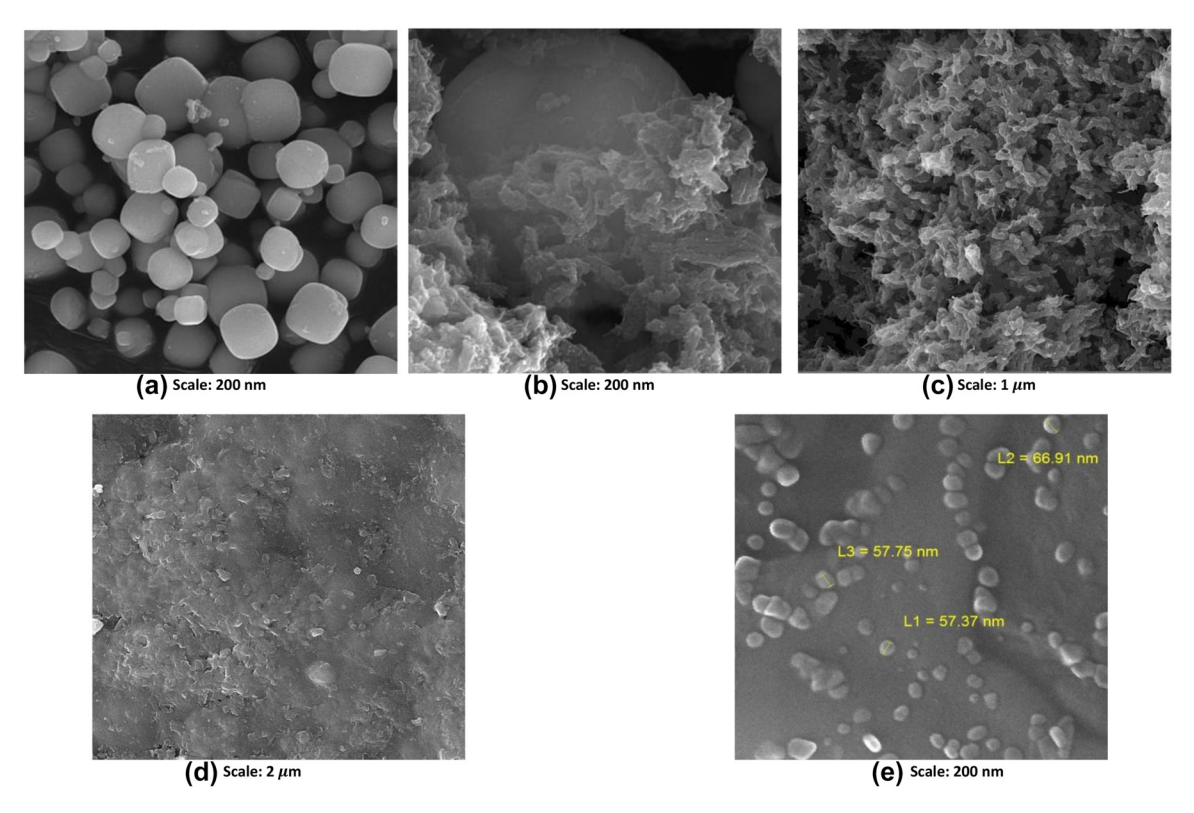


Figure 2: FESEM images of (a) cobalt ferrite in 500 nm, (b) cobalt ferrite/polyaniline in 200 nm, (c) cobalt ferrite /polyaniline/graphite in 1 μm, (d) cobalt ferrite /polyaniline/graphite/thermoplastic polyurethane composites in 2 μm, and (e) cobalt ferrite /polyaniline/graphite/thermoplastic polyurethane composites in 200 nm.

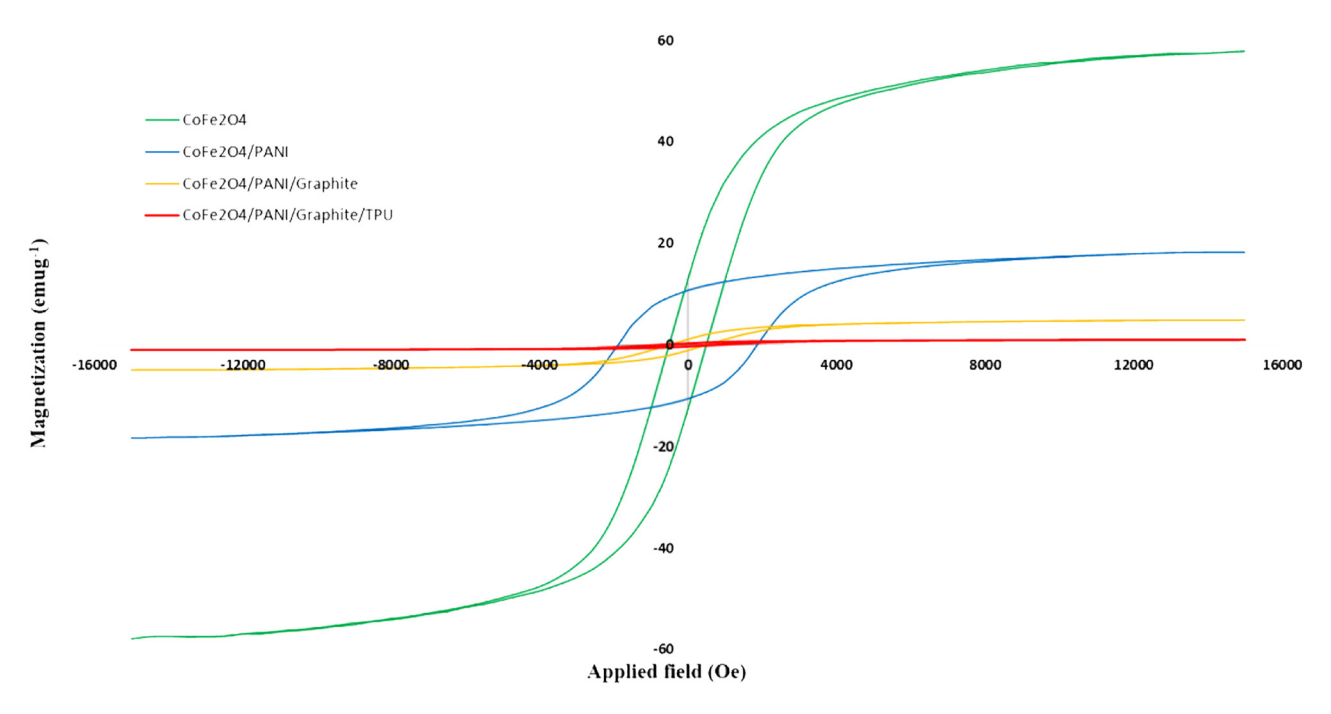


Figure 3: The magnetic hysteresis loops of (a) cobalt ferrite, (b) cobalt ferrite /polyaniline, (c) cobalt ferrite /polyaniline/graphite, and (d) cobalt ferrite /polyaniline/graphite/thermoplastic polyurethane composites.

coercivity was 737 Oe. TPU also decresed magnetic saturation. TPU is a non-magnetic material, so it further decreases magnetic saturation.

3.4 Water absorption – environmental stability against humidity

Water absorption in composites causes damage and disorder communication between the matrix and fillers. It thus decrases mechanical properties (tensile strength, impact resistance). It also changes the form of composites (swelling caused by water absorption). Also, water in a material affects its electrical properties, thermal performance, and dielectric properties.

ASTM D570 is one of the most commonly used standard methods for measuring water absorption in polymers. This method was performed on composites at room temperature and in humid conditions. First, the samples were placed in an oven for 24 h at 50 °C and then in a dryer to cool. Immediately after cooling, the samples were weighed. Then, the samples were immersed in water at 23 °C for 24 h. After that, the samples were dried with a lint-free cloth and weighed again. Finally, the percentage of water absorption was calculated by Equation (1) [33]:

Water absorption =
$$[(w_2 - w_1)/w_1] \times 100$$
 (1)

Here, w_1 is the weight of the sample after drying in the oven, and w_2 is the weight after immersion in water.

Table 1 shows the percentage of water absorption for pure TPU (matrix), pure PANI, and composites.

Table 1 shows the water absorption percentage of two pure thermoplastic materials, TPU and PANI. The results show that TPU was hydrophobic, and PANI was hydrophobic

Table 1: Water absorption percentage in samples with a thickness of 1.5 mm.

Composite	Graphite	Polyaniline	CoFe ₂ O ₄	TPU	Water
no	(%)	(%)	(%)	(%)	absorption (%)
Pure TPU					0.42
Pure PANI					2.54
3	5	15	6	74	5.15
10	5	20	2	73	5.21
5	10	15	2	73	5.55
2	5	25	6	64	6.08
24	5	20	10	65	6.34
16	10	25	2	63	6.94
8	10	15	10	65	7.05
12	10	20	6	64	7.19
6	15	15	6	64	7.25
9	15	20	2	63	7.78
7	10	25	10	55	8.82
17	15	25	6	54	9.94
13	15	20	10	55	10.28

with less intensity. For various composites, an inverse relationship was shown between the water absorption percentage and the weight percentage of TPU. Results reveal that the G in composites shows a hydrophilic property, confirming a previous report [34]. The effect of G on water absorption in composites causes layered structure and porosity.

On the other hand, for similar concentrations (wt.%) of G and TPU, the weight changes of PANI due to water absorption percentage were noticeable (sample no. 12 with 8). However, samples 2 and 24 showed an increased PANI wt.% (20–25) with a decreasing percentage of water absorption. That can be attributed to water molecules absorbed through the hydrogen bonds of PANI. Additionally, groups such as –OH and –COOH in the composite are important for water absorption, increasing the weight percent PANI by up to 20 % increased water absorption. However, a further increase in PANI from 20 % led to accumulation and restraint of water uptake.

3.5 Thermogravimetric analysis – thermal stabilities of the composite

Thermal gravimetric analysis (TGA) is a method used to evaluate a material's thermal stability. All samples were heated in air to 800 °C at 10 K min⁻¹. The weight loss percentages of the samples with temperature are shown in

Figure 4. All the samples had the same thickness (2 mm) and constituents such as CF, TPU, PANI, and G.

The curves of CF show weight loss in two steps. The first weight loss occurred at 50-125 °C, which was related to the evaporation of water absorbed on the surface of the CF. In stage 2, the weight loss was steady, ranging from 150 to 400 °C. From 500 to 800 °C, the slope of the curve remains constant. CF has thermal stability of up to 800 °C. The TGA curve of G showed negligible weight loss up to 800 °C. Graphite was thermally stable at temperatures less than 800 °C. The TGA curve of PANI shows that weight loss occurs in three stages. The first zone, up to 130 °C, showed a modest drop in weight, which might be attributed to the water molecule and dopant (HCl) loss from the PANI chains. The second zone, which ranged from 130 to 230 °C, was where functional groups (-COOH) were lost. In this area, the polymer had thermal stability. The third area related to continuous weight loss from 230 to 550 °C was the breakdown of the polymer skeleton at 600-800 °C, a slope of zero related to the residual PANI. The maximum thermal stability of PANI was recorded at 230 °C.

Thermal decomposition of TPU occurred in three steps. In the first stage, moisture was evaporated at up to 100 °C. The second stage took place at around 300 °C, and the third stage was at 410 °C.

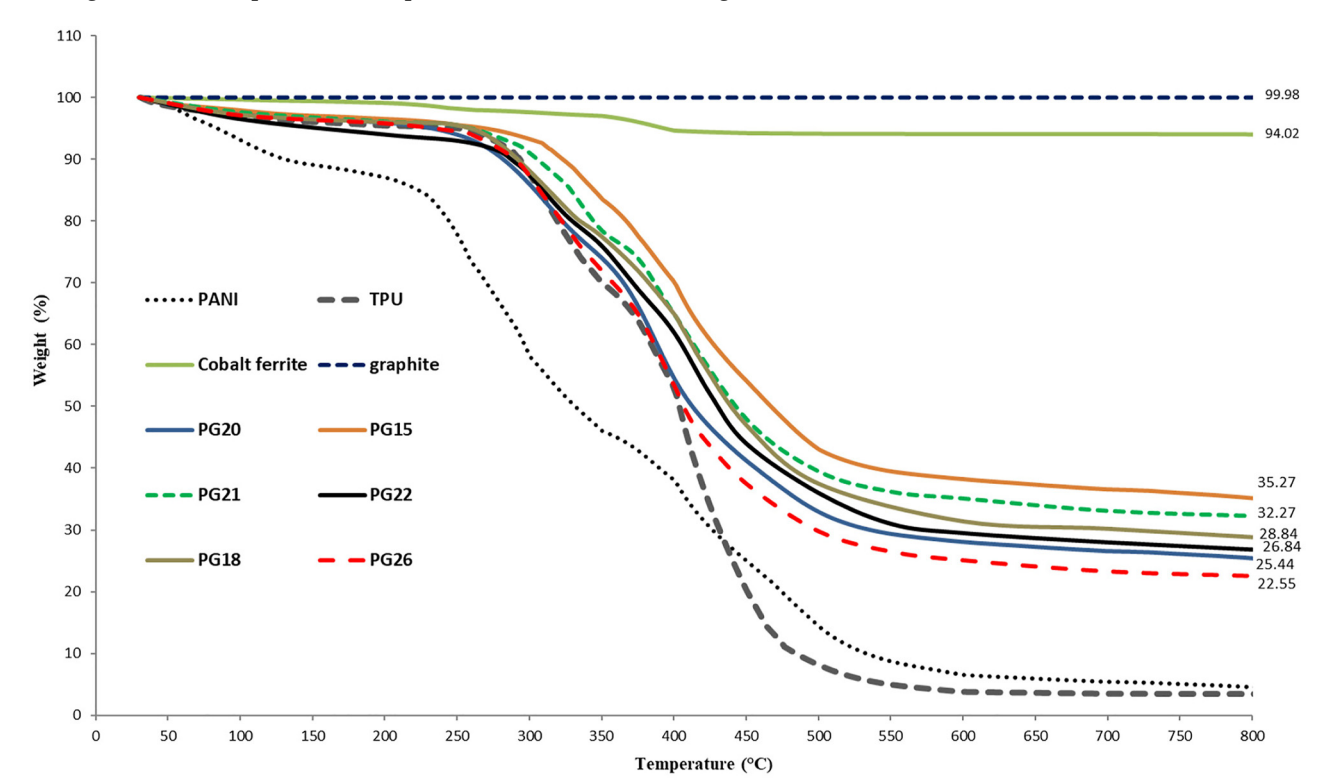


Figure 4: TGA curve of 6 composites at a thickness of 2 mm and cobalt ferrite, graphite, polyaniline and thermoplastic polyurethane.

Destruction in steps 2 and 3 was due to urethane decomposition in the hard part and polyol decomposition in the soft part of TPU. Step 2 involves separating urethane from the primary polyol and isocyanate. In step 3, the polyol was destroyed [35, 36]. At 500 °C, the slope of the curve decreased to near zero, indicating that the polymer had been destroyed, leaving only the remaining carbon. Between 600 and 800 °C, TPU recorded the remaining percentage (3.5 %). Pure TPU remained stable up to 290 °C. Almost all composites decomposed at 260-450 °C, and the remaining components were G and CF. Sample no. 15 had the highest thermal stability at 310 °C and the highest residual weight of 35.27 %, followed by samples no. 21, 18, 22, 20, and 26, in that order. The results showed that adding fillers, G, and CF to the matrix increased the composites' thermal stability. Compared to the curves of samples no. 18 and 22, increasing the percentage of PANI decreses thermal stability. The form of the curves was similar to that of pure TPU for composites with a more significant TPU weight percentage. They were also thermally stable between 260 and 310 °C.

3.6 D.C. Electrical conductivity

The electrical conductivity test was performed on composite films (1.5 mm in thickness) at room temperature. The results are shown in Table 2.

The weight percent of G in films is nearly directly linked with the increase in electrical conductivity. The electrical conductivities of pure TPU, CF, PANI, and G were 10⁻¹³, 8 \times 10⁻⁹, 4.1, and 352. TPU was almost an electrical insulator, and CF was almost non-conductive. The conductivity of the guaternary composites varied from 18.9 to 78.9 S cm⁻¹.

Table 2: Electrical conductivity in samples with a thickness of 1.5 mm.

Material no	Graphite (%)	Polyaniline (%)	CoFe ₂ O ₄ (%)	TPU (%)	Conductivity (s/cm)
10	5	20	2	73	18.87
3	5	15	6	74	25.14
5	10	15	2	73	28.08
9	15	20	2	63	42.25
24	5	20	10	65	25.48
8	10	15	10	65	27.93
12	10	20	6	64	32.30
11	10	20	6	64	32.30
16	10	25	2	63	30.07
14	10	20	6	64	32.30
7	10	25	10	55	57.57
17	15	25	6	54	81.17
2	5	25	6	64	52.42
13	15	20	10	55	76.89
6	15	15	6	64	78.89

PANI placement in the space between the G layers has a synergistic effect. PANI acts as an electron donor and G as an electron acceptor [37]. Therefore, when exposed to a different potential, the separated electrons move freely, leading to a significant increase in electrical conductivity. With 15 wt.% G and 15-20 wt.% of PANI, about 22 % of the conduction of pure G was achieved (despite the electrical resistance of TPU in the composite matrix). When CF was combined with G. an interaction was created: CF was converted from an insulator to a semiconductor. According to Table 2, when the wt.% of CF increased composites no. 12 and 16, the electrical conductivity increased.

3.7 Principles of electromagnetic interference (EMI) shielding theory

The EMI SE theory is defined as the shielding restraint of propagating EM waves. The shielding effectiveness of a material is determined by the decrease of the magnetic or electric field caused by shielding. Each shielding material decreses EM radiation through three mechanisms. The sum of the three, reflection, absorption, and multiple internal reflections, defines SE_T and is given by Equation (2):

$$SE_{\rm T} = SE_{\rm R} + SE_{\rm A} + SE_{\rm M} \tag{2}$$

When SE_T is greater than 15 dB, SE_M can be ignored, and Equation (3) results [38]:

$$SE_{\rm T} = SE_{\rm R} + SE_{\rm A} \tag{3}$$

Shielding efficacy is the ratio of power received with and without material for the same incoming power. It is represented in decibels and is computed as follows [39]:

$$SE = -10 \log P_1/P_2 \tag{4}$$

Here, P_1 is the electromagnetic power before installing the shield, P_2 is the same quantity after installing the shield, and both are measured at the same point. A shielding effectiveness of 10 dB equals 90 % of reflected or absorbed electromagnetic energy. To achieve 99.9 % EM energy reflection or absorption by a medium, a minimum of 20 dB SE is required [40]. According to another assessment, 30 dB for SE is suitable for 50 % of applications in the automotive and computer industries [41]. Another study [42] suggests an SE of 20 for general use. According to previous research [43], an EMI SE of 20 dB is suitable for commercial use, matching a transmission of less than 1 % of the EM wave. Another study [38] found that SE with 30 dB matching and 99.9 % wavelength weakening is deemed high for SE applications. Term SE_{T} is described as a reflection, absorption, and multiple reflections [44].

In the military field, $SE_{\rm T}$ values of EMI shielding materials of at least 30 dB are needed [45]. A $SE_{\rm T}$ equivalent to 20 dB is appropriate for various electronic applications [46–48]. According to the relations and values of the S parameters of the network analyzer, transmission (T), reflection (R), and absorption (A) are calculated using Equations (5)–(7) [49, 50]:

$$T = S_{12}^{2} = S_{21}^{2} \tag{5}$$

$$R = S_{11}^2 = S_{22}^2 \tag{6}$$

$$A = 1 - R - T \tag{7}$$

Therefore, the shielding mechanisms by reflection (SE_R) and absorption (SE_A) are defined by Equations (8)–(10) [51]:

Absorption loss(
$$SE_A$$
) = $10 \log_{10} \left(\frac{1 - |S_{11}|^2}{|S_{12}|^2} \right)$ (8)

Reflection loss
$$(SE_R) = 10 \log_{10} \left(\frac{1}{1 - |S_{11}|^2} \right)$$
 (9)

Total shielding
$$(SE_T) = SE_A + SE_R = -20 \log_{10} |S_{21}|$$
 (10)

 S_{11} , S_{22} , S_{12} , and S_{21} are the input reflection coefficient, output reflection coefficient, reverse gain coefficient, and forward gain coefficient.

The effectiveness of the EMI shielding (dB) with the following Equation converted to the EMI shielding efficiency (%) [52]:

shielding efficiency (%) =
$$100 - \left(\frac{1}{10^{\frac{SE}{10}}}\right) \times 100$$
 (11)

3.8 EMI shielding properties and mechanism

According to previous research, $SE_{\rm T}=30~{\rm dB}$ was deemed ideal. We constructed twenty-seven film composites with 1, 1.5, and 2 mm thicknesses. We calculated the $SE_{\rm T}$ using the S parameters of the VNA by Equation (10); the results are given in Figure 6a–c.

As shown in Figure 5a, the ideal sample is composite film no. 4 with $SE_{\rm T}=30.7$. Because Sample no. 1 comprised the lowest weight percentages of PANI and $SE_{\rm T}$, composites containing less than 20 % PANI are not acceptable for shielding at a 1 mm thickness. When samples no. 27 and no. 4 are compared, the effect of G weight gain and CF weight loss on increasing $SE_{\rm T}$ from 26.8 to 30.7 is evident. Increasing PANI's weight to greater than 20 % did not substantially raise $SE_{\rm T}$ (samples no. 23 and 4). Also, the change in the $SE_{\rm T}$ was the opposite of the change in the weight percent of the matrix TPU.

In Figure 5b, at a thickness of 2 mm, sample no. 14 with $SE_T = 30.1$ was selected as the optimal sample. Also,

the highest SE_T was related to no. 6. Because of the more significant interaction of materials, the electrical conductivity of sample no. 6 was higher than that of sample no. 13. When samples no. 6 and 9 are compared, the binding effect of CF as a magnetic material in increasing SE_T is observed.

In Figure 5c, sample no. 18 with $SE_{\rm T}=30.1$ was selected as the optimal sample. Sample no. 15, with $SE_{\rm T}=47.9$, received the highest $SE_{\rm T}$ and best performance. When comparing samples 26 and 15, raising the G of weight percent from 5 to 10 and decreasing the weight percent TPU increased $SE_{\rm T}$ from 25.5 to 47.9.

Numerous studies have revealed that absorption loss on $SE_{\rm T}$ is significantly greater than reflection loss and plays a critical impact. In several investigations [53, 54] absorption loss ranged between 75 and 85 % of $SE_{\rm T}$. Composites with high electrical conductivity and high $SE_{\rm A}$ are used in stealth technology.

Therefore, the following shows the change of absorption loss with frequency in the X-band; at a thickness of 1 mm, none of the samples had an absorption loss of more than 30 dB, so they were not chosen for specialized and advanced uses.

The maximum absorption loss at 1.5 mm thickness was 35.6 dB (samples no. 6), adequate for stealth technology. The sample with the lowest absorption loss (sample no. 10) had a loss of 75 %, while the sample with the highest loss had a loss of 92 % (sample no. 13).

At a thickness of 2 mm, samples no. 21, 22, and 15 exhibited absorption losses of 31.4, 37.5, and 45 dB, respectively, adequate for advanced applications. The sample with the lowest absorption loss (82 %) was sample no. 20, whereas the sample with the highest absorption loss (96 %) was sample no. 22.

The changes in absorption loss at different thicknesses in different samples were such that at a thickness of 1 mm, the maximum absorption loss was 81%. The minimum absorption loss was 72%, and at a thickness of 1.5 mm, the maximum absorption loss was 92%. The minimum absorption loss was 75%, and at a thickness of 2 mm, the maximum absorption loss was 96%, and the minimum absorption loss was 89%, which indicates the effect of extreme thickness on the increase in the amount of absorption pressure on the reflection loss. It is important to remember that the reflection loss is determined according to Equation (3) by the values left at 100%. The relationship between SE_T and SE_A in the X-band is given in Figure S2.

Because CF had magnetic characteristics, the change in the weight percent of CF was substantial for two samples of the same thickness.

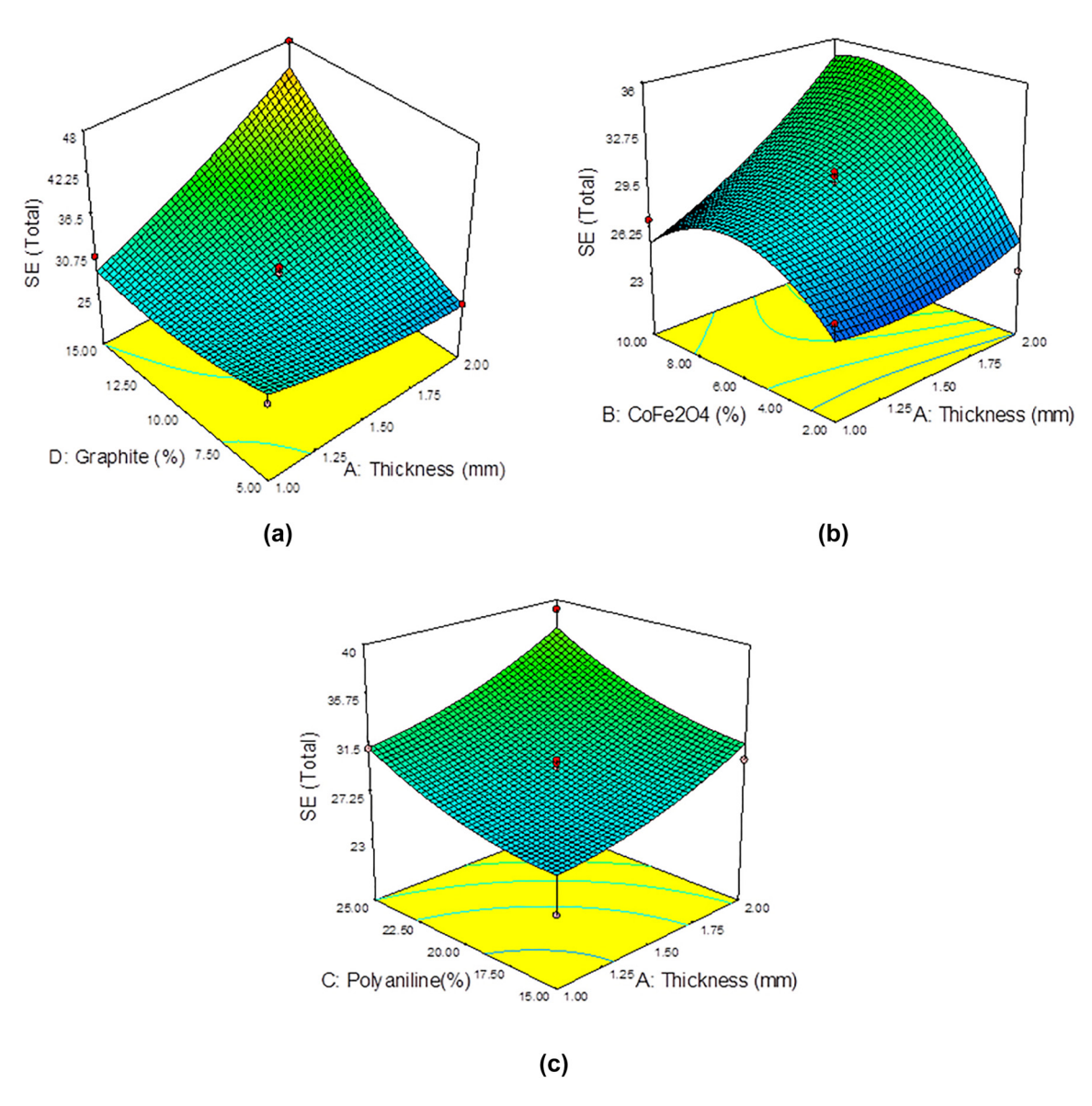


Figure 5: The relationship between to weight percentage of materials and SE, at thickness: (a) 1 mm, (b) 1.5 mm, and (c) 2 mm.

At 10 GHz (composites 13 and 21), the percentage absorption loss rose, as did the percentage absorption loss above 10.5 GHz (composites no. 15 and 22). $SE_{\rm T}$ was more than 30 dB across the whole frequency range X, showing that four composites are better for use in industrial applications.

3.9 Response surface methodology

The response surface methodology (RSM) collects statistical techniques used to optimize, affecting several variables' responses. This strategy minimizes the number of experiments and allows for the estimation of all second-order regression model coefficients and interacting components.

This study examined the relationship between the earned responses and variables. We have also optimized variables by the surface response method with Box Behnken Design (BBD) of Design-Expert software. The effects of independent variables such as percentage by weight of $CoFe_2O_4$ (levels 2, 6, 10), PANI (levels 15, 20, 25), G (levels 5, 10, 15), and the thickness of three levels (1, 1.5, 2 mm) on SE_T (as response) were investigated. In total, 27 samples were tested.

Finally, data were entered into the Design-Expert software to determine and achieve the best thickness, composition, and weight percent to achieve an ideal composite. Based on how the software set up the tests, the highest value was $SE_T = 47.9$ dB.

According to the ANOVA table, the R-squared and adj R-squared values were equal to 0.9086 and 0.8020, respectively, and showed the model's accuracy. First, the wt.% of G, then the thickness of the composite, then the wt.% of CF, and finally the wt.% of PANI affected the SE_{T} .

A second-order multivariate Equation was obtained according to the obtained results, which showed the experimental relationship between the tested variables and SE_{T} . The results of the variance analysis for the quadratic response level model on the experimental data are shown in Table 3.

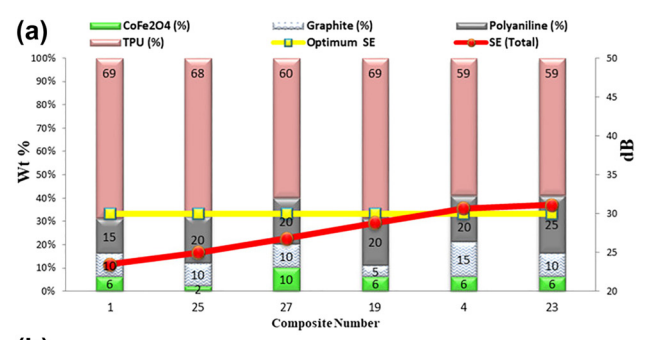
Shielding Efficiency (Total) = $29.70 + (2.75 \times A) + (2.70$ $\times B$) + (2.58 \times C) + (4.34 \times D) + (2.02 \times A \times B) + (0.35 \times A \times $(C) + (5.13 \times A \times D) - (0.22 \times B \times C) + (0.80 \times B \times D) - (4.55)$ $\times C \times D$) + $(0.94 \times A^2)$ - $(3.34 \times B^2)$ + $(1.10 \times C^2)$ + $1.52 \times D^2$

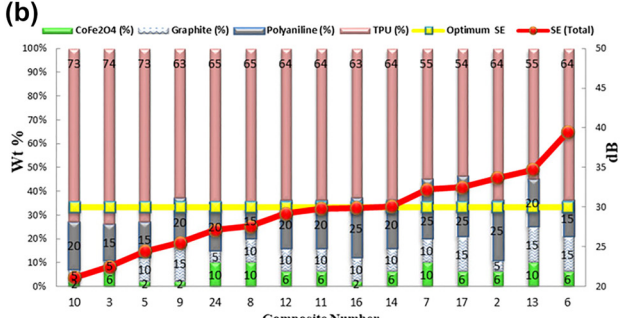
Figure 6a shows the effect of wt.% CF on total shielding. SE_{T} increased with CF in the 2 to 7 wt.% range and then declined. This effect is evident in the SE_{T} change from 25.4 to 33.1 dB based on data from the ANOVA (Table 3), which shows that thickness and then wt.% of the CF effectively increased SE_{T} .

Figure 6b shows the effect of wt.% PANI on total shielding. SE_T increased with wt.% of PANI, especially in the 20 to 25 wt.% range. This effect is evident in the SE_T change from 28.5 to 35.6 dB. From a comparison of the slopes of Figures 6a and b, the difference between the effects of CF and PANI was noticeable.

Table 3: Analysis of variance (ANOVA) for response surface guadratic model for different agents.

Source	Sum of squares	Degree of freedom	Mean square	<i>F</i> -value	<i>P</i> -value prob > <i>F</i>
Model	815.89	14	58.28	8.52	0.0003
A-thickness	90.75	1	90.75	13.27	0.0034
B-CoFe ₂ O₄	87.48	1	7.48	12.79	0.0038
C-polyaniline	79.57	1	79.57	11.64	0.0052
<i>D</i> -graphite	226.20	1	226.20	33.08	< 0.0001
AB	16.40	1	16.40	2.40	0.1474
AC	0.49	1	0.49	0.072	0.7935
AD	105.06	1	105.06	15.36	0.0020
BC	0.20	1	0.20	0.030	0.8662
BD	2.56	1	2.56	0.37	0.5520
CD	82.81	1	82.81	12.11	0.0045
A^2	4.69	1	4.69	0.69	0.4239
B^2	59.41	1	59.41	8.69	0.0122
C ²	6.45	1	6.45	0.94	0.3505
D^2	12.40	1	12.40	1.81	0.2029
Residual	82.05	12	6.84		
Lack of fit	81.63	10	8.16	38.87	0.0553
Pure error	0.62	2	0.21		





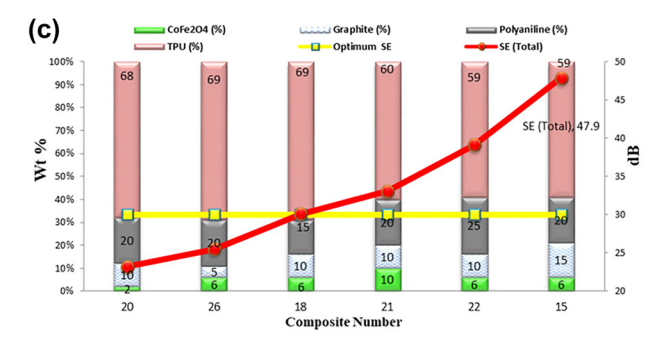


Figure 6: Response surface plot of interacting effects of cobalt ferrite, polyaniline, and graphite on SE_{τ} .

Figure 6c shows the effect of wt.% G on total shielding. $SE_{\rm T}$ increased with G in the 7.5 to 15 wt.% range. The effect of graphite on $SE_{\rm T}$ was outstanding, from 28.6 to 41.2 dB.

Software output shows the different values of the optimal film composite FM scroll file placed in the below path . According to the thickness of 1.26 mm, the weight percentages of CF, PANI, and G were 6.95 %, 20.04 %, and 12.13 %, respectively, to achieve the minimum value of $SE_T = 30$. Also, the weighted TPU was 60.88 %.

4 Conclusions

A composite film was used as an electromagnetic wave absorbing coating. It consisted of CF as a magnetic material, graphite, and PANI as dielectric and conductive materials, respectively, and TPU with good mechanical and thermal properties. The composite had good stability in humid conditions and achieved thermal stability up to 310 °C. The roles of graphite and CF in thermal stability and TPU in reducing water absorption were noticeable.

The synergy of graphite and PANI was significant in increasing the electrical conductivity. Increased electrical conductivity improved electromagnetic absorption significantly. The SE_A was an important factor in SE_T , especially at 10-12 GHz frequencies. Firstly, the thickness of the composite and then the CF content had tremendous effects on increasing the SE_{Δ} .

A composite with an optimal combination of 4 materials to achieve an $SE_T > 30$ dB with a thickness of 1.26 mm was obtained. In one of the samples, the maximum SE_{T} averaged 47.9 dB with a thickness of 2 mm in the X-band.

Finally, it was shown that quaternary nanocomposites have many advantages in absorbing electromagnetic waves. However, it was very complicated and essential to optimize them due to the interaction of materials. This film composite can be used for industrial applications and stealth military equipment from radar because it has a very high SE_T in all X-band and is very light and thin. It is suggested that more research be done on the usage of graphite in composites with military applications that need $SE_{\rm T} > 35$.

Author contributions: All the authors have accepted responsibility for the entire content of this submitted manuscript and approved submission.

Research funding: None declared.

Conflict of interest statement: The authors declare no conflicts of interest regarding this article.

References

- 1. Choi J., Nam Y., Jang M., Kim C. Compos. Struct. 2018, 202, 290. https://doi.org/10.1016/j.compstruct.2018.01.081.
- 2. Yang H., Ye T., Lin Y., Zhu J., Wang F. J. Alloys Compd. 2016, 683, 567. https://doi.org/10.1016/j.jallcom.2016.05.127.
- 3. Singh S. K., Akhtar M. J., Kar K. K. ACS Appl. Mater. Interfaces 2018, 10, 24816. https://doi.org/10.1021/acsami.8b06673.
- 4. Chamoli P., Singh S. K., Akhtar M., Das M. K., Kar K. K. Phys. E 2018, 103, 25. https://doi.org/10.1016/j.physe.2018.05.020.
- 5. Kim H. G., Shin H. J., Kim G. C., Park H. J., Moon H. J., Kwac L. K. Carbon Lett. 2014, 15, 268. https://doi.org/10.5714/CL.2014.15.4.268.
- 6. do Amaral Junior M. A., Marcuzzo J. S., da Silva Pinheiro B., Lopes B. H. K., de Oliveira A. P. S., Matsushima J. T., Baldan M. R. J. Mater. Res. Technol. 2019, 8, 4040. https://doi.org/10.1016/j.jmrt.2019.07
- 7. González M., Pozuelo J., Baselga J. J. Chem. Rec. 2018, 18, 1000. https://doi.org/10.1002/tcr.201700066.
- 8. Mingdong C., Huangzhong Y., Xiaohua J., Yigang L. J. Appl. Surf. Sci. 2018, 434, 1321. https://doi.org/10.1016/j.apsusc.2017.11 .107.

- 9. Ren F., Guo Z., Shi Y., Jia L., Qing Y., Ren P., Yan D. J. J. Alloys Compd. 2018, 768, 6. https://doi.org/10.1016/j.jallcom.2018.07.209.
- 10. Özerol E. A., Şenkal B., Okutan M. J. Microelectron. Eng. 2015, 146, 76. https://doi.org/10.1016/j.mee.2015.03.062.
- 11. Wu X., Qi S., He J., Duan G. J. J. Mater. Sci. 2010, 45, 483. https://doi .org/10.1007/s10853-009-3965-y.
- 12. Sun J., Xu H., Shen Y., Bi H., Liang W., Yang R. B. J. Alloys Compd. 2013, 548, 18. https://doi.org/10.1016/j.jallcom.2012.08.114.
- 13. Singh V. K., Shukla A., Patra M. K., Saini L., Jani R. K., Vadera S. R., Kumar N. J. Carbon 2012, 50, 2202. https://doi.org/10.1016/j.carbon .2012.01.033.
- 14. Wang S., Zhao Y., Xue H., Xie J., Feng C., Li H., Shi D., Muhammad S., Jiao Q. J. Mater. Lett. 2018, 223, 186. https://doi.org/10.1016/j .matlet.2018.04.050.
- 15. Hapishah A., Syazwan M., Hamidon M. J. J. Mater. Sci. 2018, 29, 20573. https://doi.org/10.1007/s10854-018-0192-9.
- 16. Chen W., Zhu X., Liu Q., Fu M. J. M. L. Mater. Lett. 2017, 209, 425. https://doi.org/10.1016/j.matlet.2017.08.075.
- 17. Bourdo S., Li Z., Biris A. S., Watanabe F., Viswanathan T., Pavel I. J. Adv. Funct. Mater. 2008, 18, 432. https://doi.org/10.1002/adfm .200700425.
- 18. Chen K., Xiang C., Li L., Qian H., Xiao Q., Xu F. J. J. Mater. Chem. 2012, 22, 6449. https://doi.org/10.1039/C2JM15096D.
- 19. Gulzar N., Zubair K., Shakir M. F., Zahid M., Nawab Y., Rehan Z. J. Supercond. Novel Magn. 2020, 33, 3519. https://doi.org/10.1007/ s10948-020-05608-w.
- 20. Shukla V. J. J. O. M. S. J. Mater. Sci. 2020, 55, 2826. https://doi.org/10 .1007/s10853-019-04198-w.
- 21. Bertolini M., Ramoa S., Merlini C., Barra G., Soares B., Pegoretti A. Front. Mater. 2020, 7, 174. https://doi.org/10.3389/fmats.2020 .00174.
- 22. Vaid K., Chaurasia A., Rathore D., Singhal R., Dwivedi U. Polym. Compos. 2021, 42, 819. https://doi.org/10.1002/pc.25867.
- 23. Zhu X., Wang X., Liu K., Yuan H., Boudaghi R., Akhtar M. N. J. Alloys Compd. 2021, 873, 159818. https://doi.org/10.1016/j.jallcom.2021
- 24. Cao Y., Farouk N., Mortezaei N., Yumashev A. V., Akhtar M. N., Arabmarkadeh A. Ceram. Int. 2021, 47, 12244. https://doi.org/10 .1016/j.ceramint.2021.01.073.
- 25. Gang Q., Akhtar M. N., Boudaghi R. J. Magn. Magn Mater. 2021, 537, 168181. https://doi.org/10.1016/j.jmmm.2021.168181.
- 26. Zhao S., Ma D., Jin W. J. J. Nanomater. 2010, 2010, 28. https://doi .org/10.1155/2010/842816.
- 27. Divya K., Chandran A., Reethu V., Mathew S. J. A. S. S. Appl. Surf. Sci. 2018, 444, 811. https://doi.org/10.1016/j.apsusc.2018.01
- 28. Hadi A., Zahirifar J., Karimi J., Dastbaz A. J. Ultrason. Sonochem. 2018, 44, 204. https://doi.org/10.1016/j.ultsonch.2018.02.028.
- 29. Liu H., Dong M., Huang W., Gao J., Dai K., Guo J., Zheng G., Liu C., Shen C., Guo Z. J. J. Mater. Chem. C 2017, 5, 73. https://doi.org/10 .1039/C6TC03713E.
- 30. Kooti M., Afshari M. J. Sci. Iran. 2012, 19, 1991. https://doi.org/10 .1016/j.scient.2012.05.005.
- 31. Prasanna G., Jayanna H., Lamani A., Dash S. J. Synth. Met. 2011, 161, 2306. https://doi.org/10.1016/j.synthmet.2011.08.039.
- 32. Zhang K., Zhang J., Ma L., Liang Y., Yang X., Cui Z., Zhu S., Li Z. J. Design: Mater. Des. 2018, 143, 169. https://doi.org/10.1016/j.matdes .2018.01.036.

- 33. Gupta M. K., Srivastava R., Kumar S., Gupta S., Nahak B. J. Am. J. Polym. Sci. Technol. 2015, 3, 208.
- 34. Kozbial A., Zhou F., Li Z., Liu H., Li L. J. Acc. Chem. Res. 2016, 49, 2765. https://doi.org/10.1021/acs.accounts.6b00447.
- 35. Kanbur Y., Tayfun U. J. Thermoplast. Compos. Mater. 2018, 31, 1661. https://doi.org/10.1177/0892705717743292.
- 36. Dong M., Li Q., Liu H., Liu C., Wujcik E. K., Shao Q., Ding T., Mai X., Shen C., Guo Z. *Polymer* 2018, 158, 381. https://doi.org/10.1016/j .polymer.2018.11.003.
- 37. Saini P., Choudhary V., Dhawan S. Indian J. Eng. Mater. Sci. 2007, 14,
- 38. Yan D. X., Pang H., Li B., Vajtai R., Xu L., Ren P. G., Wang J. H., Li Z. M. Adv. Funct. Mater. 2015, 25, 559. https://doi.org/10.1002/adfm .201403809.
- 39. Gültekin B. C., Gültekin N. D., Atak O., Şimsek R. Fibers Polym. 2018, 19, 313. https://doi.org/10.1007/s12221-018-7462-7.
- 40. Janda N. B., Keith J. M., King J. A., Perger W. F., Oxby T. J. J. Appl. Polym. Sci. 2005, 96, 62. https://doi.org/10.1002/app.
- 41. Yang S., Lozano K., Lomeli A., Foltz H. D., Jones R. Composites, Part A 2005, 36, 691. https://doi.org/10.1016/j.compositesa.2004.07
- 42. Gupta A., Choudhary V. Compos. Sci. Technol. 2011, 71, 1563. https:// doi.org/10.1016/j.compscitech.2011.06.014.
- 43. Al-Saleh M. H., Saadeh W. H., Sundararaj U. Carbon 2013, 60, 146. https://doi.org/10.1016/j.carbon.2013.04.008.
- 44. Al-Saleh M. H., Sundararaj U. Carbon 2009, 47, 2. https://doi.org/10 .1016/j.carbon.2008.09.039.

- 45. Wang H., Wang G., Li W., Wang Q., Wei W., Jiang Z., Zhang S. J. J. Mater. Chem. 2012, 22, 21232. https://doi.org/10.1039/ C2IM35129C.
- 46. Tantawy H. R., Aston D. E., Smith J. R., Young J. L. ACS Appl. Mater. Interfaces 2013, 5, 4648. https://doi.org/10.1021/am401695p.
- 47. Al-Saleh M. H., U.J. Sundararaj Carbon 2009, 47, 1738. https://doi .org/10.1016/j.carbon.2009.02.030.
- 48. Gill N., Sharma A. L., Gupta V., Tomar M., Pandey O., Singh D. P. J. J. O. A. J. Alloys Compd. 2019, 797, 1190. https://doi.org/10.1016/j .jallcom.2019.05.176.
- 49. Saini P., Arora M. J. New Polymers for Special Applications; InTechOpen, Vol. 3, 2012; p. 73.
- 50. Bayat M., Yang H., Ko F., Michelson D., Mei A. J. P. Polymer 2014, 55, 936. https://doi.org/10.1016/j.polymer.2013.12.042.
- 51. Al-Saleh M. H., Saadeh W. H., Sundararaj U. J. C. Carbon 2013, 60, 146. https://doi.org/10.1016/j.carbon.2013.04.008.
- 52. Lee J., Liu Y., Park S., Park M., Kim H. J. Mater. Chem. C 2017, 5, 7853. https://doi.org/10.1039/C7TC02074K.
- 53. Joshi A., Bajaj A., Singh R., Alegaonkar P., Balasubramanian K., Datar S. J. Nanotechnology 2013, 24, 455705. https://doi.org/10 .1088/0957-4484/24/45/455705.
- 54. Farhan S., Wang R., Li K. J. C. I. Ceram. Int. 2016, 42, 11330. https:// doi.org/10.1016/j.ceramint.2016.04.054.

Supplementary Material: The article contains supplementary material (https://doi.org/10.1515/ijmr-2021-8516).